# Carbon Nanotube/Silica Coaxial Nanocable as a Three-Dimensional Support for Loading Diverse Ultra-High-Density Metal Nanostructures: Facile Preparation and Use as Enhanced Materials for Electrochemical Devices and SERS

Shaojun Guo, Jing Li, Wen Ren, Dan Wen, Shaojun Dong, and Erkang Wang*

*State Key Laboratory of Electroanalytical Chemistry, Changchun Institute of Applied Chemistry, Chinese Academy of Sciences, Changchun, Jilin 130022, China, and Graduate School of the Chinese Academy of Sciences, Beijing, 100039, China*

*Received February 2, 2009. Revised Manuscript Received March 29, 2009*

In this paper, we have reported a very simple strategy (combined sonication with sol−gel techniques) for synthesizing well-defined silica-coated carbon nanotube (CNT) coaxial nanocable without prior CNT functionalization. After functionalization with $NH_2$ group, the CNT/silica coaxial nanocable has been employed as a three-dimensional support for loading ultra-high-density metal or hybrid nanoparticles (NPs) such as gold NPs, Au/Pt hybrid NPs, Pt hollow NPs, and Au/Ag core/shell NPs. Most importantly, it is found that the ultra-high-density Au/Pt NPs supported on coaxial nanocables (UASCN) could be used as enhanced materials for constructing electrochemical devices with high performance. Four model probe molecules ($O_2$, $CH_3OH$, $H_2O_2$, and $NH_2NH_2$) have been investigated on UASCN-modified glassy carbon electrode (GCE). It was observed that the present UASCN exhibited high electrocatalytic activity toward diverse molecules and was a promising electrocatalyst for constructing electrochemical devices with high performance. For instance, the detection limit for $H_2O_2$ with a signal-to-noise ratio of 3 was found to be 0.3 $\mu$M, which was lower than certain enzyme-based biosensors. And the detection limit for hydrazine is $<0.5$ $\mu$M, which was lower than amperometric hydrazine sensors based on functional nanomaterials such as zinc oxide nanonails, CNTs-modified electrodes, *o*-aminophenol grafted GCE electrode, and multilayer film containing cobalt phthalocyanine. Furthermore, the as-obtained high-density gold/silver core/shell NPs supported on coaxial nanocables could be used as a good surface-enhanced Raman scattering (SERS) substrate for the detection of different molecules [4-aminothiophenol (4-ATP) and adenine], showing the great potential of CNT/$SiO_2$/(Au/Ag) as a convenient and powerful SERS substrate for biological tags and biological molecular detection.

## 1. Introduction

Coaxial nanocables, as a unique kind of one-dimensional (1D) nanoarchitecture, have drawn much attention in the last couple of decades on account of their providing the possibility of enhanced functionality and of multifunctional properties compared with those of their single-component counterparts. Many novel nanohybrids with well-defined core/shell structures such as silver or copper core in poly(vinyl alcohol) polymer,[1a,b] gold nanorod or carbon nanotube (CNT) cores in $SiO_2$,[1c−e] silicon nanowires in graphitic B−C−N nanotube,[1f] gold nanorod in polystyrene,[1g] and CNT core in $TiO_2$[1h] were just recently described. Particularly, synthesis of CNT/silica coaxial nanocables has attracted more attention on account of their numerous potential applications in science and engineering. For example, Liu and co-workers[2] reported a new method of coating single-walled carbon nanotubes with a thin layer of $SiO_2$ using 3-aminopropyltriethoxysilane as the coupling layer. Our previous report demonstrated the multistep process for synthesizing CNT/silica coaxial nanocable through the functionalization of CNTs using the polymer first.[1d] However, in all reports concerning CNT/silica coaxial nanocables, a precursor layer was needed to introduce the surface of CNTs, which makes the preparation process very complex. So it is very necessary to introduce a simple and rapid method for synthesizing silica homogeneously coated on the surface of CNTs to form well-defined coaxial nanocables.

Also, metal nanomaterials have continued to receive considerable interest because of their particular optical, electronic, and magnetic properties and their important applications in many fields such as nanosensors,[3] catalysis,[4] biomedicine,[5] biological labeling,[6] and surface-enhanced Raman scattering (SERS).[7] Functionalizing CNTs with metal NPs that combine the properties of two functional nanomaterials, such as high conductivity and surface area of CNTs and unique catalytic properties of metal NPs, to achieve a

* To whom correspondence should be addressed. E-mail: ekwang@ciac.jl.cn. Fax: +86-431-85689711.

(1) (a) Luo, L.; Yu, S.; Qian, H.; Zhou, T. *J. Am. Chem. Soc.* **2005**, *127*, 2822. (b) Zhan, Y.; Yu, S. *J. Am. Chem. Soc.* **2008**, *130*, 5650. (c) Pastoriza-Santos, I.; Pérez-Juste, J.; Liz-Marzán, L. M. *Chem. Mater.* **2006**, *18*, 2465. (d) Guo, S.; Dong, S.; Wang, E. *J. Phys. Chem. C* **2008**, *112*, 2389. (e) Guo, S.; Huang, L.; Wang, E. *New J. Chem.* **2007**, *31*, 575. (f) Zhang, Y.; Suenaga, K.; Colliex, C.; Iijima, S. *Science* **1998**, *281*, 973. (g) Obare, S. O.; Jana, N. R.; Murphy, C. J. *Nano Lett.* **2001**, *1*, 601. (h) Guo, S.; Dong, S.; Wang, E. *Small* **2008**, *4*, 1133.
(2) Fu, Q.; Lu, C.; Liu, J. *Nano Lett.* **2002**, *2*, 329.
(3) Liu, J.; Lu, Y. *J. Am. Chem. Soc.* **2003**, *125*, 6642.

10.1021/cm900300v CCC: $40.75 © 2009 American Chemical Society
Published on Web 04/29/2009

wider range of applications will therefore play an important role in the development of nanoscience and nanotechnology. As a result, considerable efforts have been directed toward covalently or noncovalently attaching certain metal NPs onto carbon nanotubes and constructing the corresponding mutilfunctional hybrid nanostructures.[8] Prominent examples include chemical binding through DNA double-helix linkages,[8a] electrochemical deposition,[8b] electroless deposition with and without the aid of reducing agents,[8c−e] and layer-by-layer technique for designing well-defined CNT/metal hybrid nanostructures.[8g] However, the low-density metal nanomaterials were supported on the surface of CNTs, which probably impact the performance of the resulting hybrid nanomaterials. Compared with the traditional methods, constructing CNT/metal hybrid nanostructures using homogeneous silica as a spacer has obvious advantages. First, a homogeneous silica shell can easily be functionalized with high-density $NH_2$ groups with a homogeneous distribution (on the surface of silica) and further lead to the loading of high-density metal NPs on the surface of the CNTs, which will provide enhanced electrocatalytic activity toward diverse small molecules. Second, CNT/silica coaxial nanocables can also be functionalized easily with other groups (e.g., SH). The functionalized coaxial nanocables can be used to adsorb high-density quantum dots (QDs) and magnetic NPs and to construct hybrid nanomaterials with novel optical and magnetic properties for electrochemical and biomedicine applications.[1h] Third, CNT/silica coaxial nanocables functionalized with metal NPs have good biocompatible properties, which probably find potential applications in biosensors and biomedicine. In this work, we have explored a facile, efficient, and economical route to obtain CNT/silica coaxial nanocables. After functionalization with $NH_2$ group, a general method has been developed for the preparation of CNT/metal NPs heterostructures with ultra-high-density metal NPs on their surfaces by using very homogeneous silica as a linker. Prominent examples include Au/Pt hybrid NPs, gold NPs, Pt hollow NPs, and Au/Ag core/shell NPs supported on the surface of CNT/silica coaxial nanocables.

As is known, the metal NPs play a key role in electrocatalytic reactions. It has been reported that metal-NPs-modified electrodes have exhibited higher electrocatalytic activities for the detection of some small molecules such as hydrazine,[9] $H_2O_2$,[10] and nitric oxide[11] than other traditional modified electrodes. More recently, many efforts have been devoted to the design of mutilfunctional metal NPs supported on 1D nanomaterials for developing high-efficiency electrochemical devices because of their higher electrochemical active area than that of individual NP.[12,13] For instance, You et al.[12] demonstrated that Pd-NPs-loaded carbon nanofibers have been employed as enhanced material for direct and mediator-less sensing $H_2O_2$ and NADH at low potentials. Yang et al.[13d] reported that three-dimensional (3D) flowerlike Pt NPs supported on CNTs exhibited high electrochemically active surface areas and were promising as electrocatalysts in direct methanol fuel cells. However, searching a general and enhanced hybrid material for constructing different electrochemical devices with high performance is still a great challenge. So it is very necessary to explore the case whether the present ultra-high-density Au/Pt NPs supported on coaxial nanocables (UASCN) can be used as enhanced materials for constructing electrochemical devices with high performance. Four model probe molecules ($O_2$, $CH_3OH$, $H_2O_2$, and $NH_2NH_2$) have been investigated on a UASCN-modified electrode. It is found that the present hybrid material exhibited high electrocatalytic activity toward diverse molecules and is a promising electrocatalyst for constructing electrochemical devices with high performance.

Also, silver nanostructures with diverse morphologies as excellent SERS substrates have gained great interest because metallic silver exhibits the best SERS effects compared to other metals such as gold and copper under certain conditions.[14] Particularly, in the case of aggregated silver NPs, interstitial gaps between adjacent nanostructures have been shown to induce intense local electromagnetic fields, known as "hot spots", upon optical excitation.[15] For instance, Dong et al.[16] developed a renewable SERS substrate prepared by cyclic depositing and stripping of silver shells on gold NP microtubes. The obtained SERS substrate containing a great number of hot spots exhibited high SERS activity. In the present work, it is interestingly found that the as-obtained high-density gold/silver core/shell NPs supported on coaxial nanocables could be used as good SERS substrates for the detection of different molecules (4-ATP and adenine) because core/shell NPs exist in the form of aggregates (containing many hot spots), showing the great potential of CNT/$SiO_2$/

(4) (a) Wang, C.; Daimon, H.; Lee, Y.; Kim, J.; Sun, S. *J. Am. Chem. Soc.* **2007**, *129*, 6974. (b) Tian, N.; Zhou, Z. Y.; Sun, S. G.; Ding, Y.; Wang, Z. L. *Science* **2007**, *316*, 732. (c) Maksimuk, S.; Yang, S.; Peng, Z.; Yang, H. *J. Am. Chem. Soc.* **2007**, *129*, 8684. (d) Sun, S. H.; Yang, D. Q.; Villers, D.; Zhang, G. X.; Sacher, E.; Dodelet, J. P. *Adv. Mater.* **2008**, *20*, 571. (e) Mahmoud, M. A.; Tabor, C. E.; El-Sayed, M. A.; Ding, Y.; Wang, Z. L. *J. Am. Chem. Soc.* **2008**, *130*, 4590.
(5) Chen, J.; Wang, D.; Xi, J.; Au, L.; Siekkinen, A.; Warsen, A.; Li, Z.-Y.; Zhang, H.; Xia, Y.; Li, X. *Nano Lett.* **2007**, *7*, 1318.
(6) Qian, X.-M.; Nie, S. M. *Chem. Soc. Rev.* **2008**, *37*, 912.
(7) (a) Banholzer, M. J.; Millstone, J. E.; Qin, L.; Mirkin, C. A. *Chem. Soc. Rev.* **2008**, *37*, 885. (b) Doering, W. E.; Piotti, M. E.; Natan, M. J.; Freeman, R. G. *Adv. Mater.* **2007**, *19*, 3100.
(8) (a) Moghaddam, M. J.; Taylor, S.; Gao, M.; Huang, S.; Dai, L.; McCall, M. J. *Nano Lett.* **2004**, *4*, 89. (b) Quinn, B.; Dekker, C.; Lemay, S. *J. Am. Chem. Soc.* **2005**, *127*, 6146. (c) Qu, L.; Dai, L. *J. Am. Chem. Soc.* **2005**, *127*, 10806. (d) Qu, L.; Dai, L.; Osawa, E. *J. Am. Chem. Soc.* **2006**, *128*, 5523. (e) Choi, H. C.; Shim, M.; Bangsaruntip, S.; Dai, H. *J. Am. Chem. Soc.* **2002**, *124*, 9058. (f) Quinn, B. M.; Dekker, C.; Lemay, S. G. *J. Am. Chem. Soc.* **2005**, *127*, 6146. (g) Yang, W.; Wang, X.; Yang, F.; Yang, C.; Yang, X. *Adv. Mater.* **2008**, *20*, 2579.
(9) Jena, B. K.; Raj, C. R. *J. Phys. Chem. C* **2007**, *111*, 6228.
(10) You, T.; Niwa, O.; Tomita, M.; Hirono, S. *Anal. Chem.* **2003**, *75*, 2080.
(11) Yu, A.; Liang, Z.; Cho, J.; Caruso, F. *Nano. Lett.* **2003**, *3*, 1203.
(12) Huang, J.; Wang, D.; Hou, H.; You, T. *Adv. Funct. Mater.* **2008**, *18*, 441.
(13) (a) Yang, D.; Sun, S.; Dodelet, J.; Sacher, E. *J. Phys. Chem. C* **2008**, *112*, 11717. (b) Mu, Y.; Liang, H.; Hu, J.; Jiang, L.; Wan, L. *J. Phys. Chem. B* **2005**, *109*, 22212. (c) Liu, Y.; Chen, J.; Zhang, W.; Ma, Z.; Swiegers, G. F.; Too, C. O.; Wallace, G. G. *Chem. Mater.* **2008**, *20*, 2603. (d) Zhao, Y.; Fan, L.; Zhong, H.; Li, Y.; Yang, S. *Adv. Funct. Mater.* **2007**, *17*, 1537. (e) Guo, S.; Dong, S. *Trends Anal. Chem.* **2009**, *28*, 96.
(14) (a) Sun, Y.; Wiederrecht, G. P. *Small* **2007**, *3*, 1964. (b) Wang, H.; Liu, C.; Wu, S.; Liu, N.; Peng, C.; Chan, T.; Hsu, C.; Wang, J.; Wang, Y. *Adv. Mater.* **2006**, *18*, 491.
(15) Wang, H.; Levin, C. S.; Halas, N. J. *J. Am. Chem. Soc.* **2005**, *127*, 14992.
(16) Wang, T.; Hu, X.; Dong, S. *Small* **2008**, *4*, 781.

(Au/Ag) as a convenient and powerful SERS substrate for biological tags and biological molecular detection.

## 2. Experimental Section

**2.1. Materials.** Multiwalled carbon nanotube (CNT, Shenzhen Nanotech Port Co., Ltd., China) with a diameter of 20−50 nm were obtained through the CVD method and purified with a 3:1 $H_2SO_4$:$HNO_3$ mixture (sonicating for 8 h). Excess acid was removed through a 450 nm polycarbonate filtration membrane. Tetraethoxysilane (TEOS), ascorbic acid (AA), uric acid (UA), $HAuCl_4 \cdot 4H_2O$, $H_2PtCl_6 \cdot 6H_2O$, $AgNO_3$, ammonium hydroxide ($NH_4 \cdot OH$), $HNO_3$, $H_2SO_4$, and ethanol were purchased from Shanghai Chemical Factory (Shanghai, China) and used as-received without further purification. 3-Aminopropyltrimethoxysilane (APTMS), 4-aminothiophenol (4-ATP), $NaBH_4$, and Nafion (perfluorinated ion-exchange resin, 5 wt % solution in a mixture of lower aliphatic alcohols and water) were obtained from Aldrich. Water used throughout all experiments was purified with the Millipore system.

**2.2. Apparatus.** A XL30 ESEM scanning electron microscope (SEM) was used to determine the morphology and composition of products. Transmission electron microscope (TEM) measurements were made on an Hitachi H-8100 EM with an accelerating voltage of 200 kV. The sample for TEM characterization was prepared by placing a drop of prepared solution on carbon-coated copper grid and dried at room temperature. X-ray photoelectron spectroscopy (XPS) measurement was performed on an ESCALAB-MKII spectrometer (VG Co., United Kingdom) with Al Kα X-ray radiation as the X-ray source for excitation. The sample for XPS characterization was dropped onto a glass slide. Electrochemical experiments were performed with a CHI 842 electrochemical workstation in a conventional three-electrode electrochemical cell using twisted platinum wire as the auxiliary electrode and Ag/AgCl as the reference electrode. The glassy carbon electrode (GCE; 3 mm) loaded with nanomaterials was employed as the working electrode. An EG&G PARC Model 366 bipotentiostat was used for rotating ring-disk electrode (RRDE) experiments. A rotating glassy carbon (GC, 5 mm) disk-platinum ring electrode was used as a working electrode. The collection efficiency ($N$) of the ring electrode obtained by reducing ferricyanide at the disk electrode was 0.139. SERS spectra were obtained on a J-Y T64000 Raman spectrometer using an Olympus microscope and a 50× long working distance objective to focus the laser beam onto a spot of about 1 $\mu m^2$. The Raman band of a silicon wafer at 520 $cm^{-1}$ was used to calibrate the spectrometer.

**2.3. Synthesis and Functionalization of CNT/Silica Coaxial Nanocables.** Two milliliters of ammonia (28 wt % in water) and 2 mL of water were added to 40 mL of a CNT ethanol solution (5 mg of CNT). After this, 0.1 mL of TEOS solution was added and sonicated for more than 8 h and kept overnight at room temperature. The resulting product was then functionalized with APTMS. Briefly, 40 uL of APTMS was added to the previous solution, followed by the addition of 1 mL of ammonia. The resulting solution was stirred for more than 12 h. Finally, the product was centrifuged (removing the excess APTMS) and further washed with ethanol and water three times, respectively, and dissolved in 10 mL of water.

**2.4. Synthesis of NPs with Different Size, Morphology, and Composition.** (a) Thirteen nanometer gold NPs were synthesized according to ref 17. One hundred milliliters of 1 mM $HAuCl_4$ was brought to a reflux while being stirred and then 10 mL of a 38.8 mM trisodium citrate solution was added quickly, which resulted in a color change of the solution from pale yellow to deep red. After the color changed, the solution was refluxed for an additional 15 min. (b) The Au/Pt hybrid NPs were synthesized via the following procedures. First, 1 wt % $HAuCl_4$ solution (1 mL) was added to 100 mL of aqueous solution. Second, 1 wt % sodium citrate (3 mL) was quickly introduced to the above solution, followed by the addition of $NaBH_4$ aqueous solution (excess). After the solution was stirred overnight, 2.5 mL of 1 wt % $H_2PtCl_6$ was added into gold NPs boiling solution, followed by the addition of 2 mL of 0.1 M AA (excess). After this solution was heated for 30 min, Au/Pt hybrid NPs were obtained. (c) Small Pt hollow spheres were synthesized via the following procedures. First, 0.25 mL of $AgNO_3$ solution (0.1 M) was added to 100 mL of aqueous solution, followed by the addition of 3 mL of sodium citrate (1 wt %). Second, $NaBH_4$ (excess) was added into the above stirring solution and placed overnight. After heating, 2.5 mL of 1 wt % $H_2PtCl_6$ was added dropwise into the above stirring solution, followed by the addition of 0.1 M AA (2 mL). After this solution was stirred for 30 min, small Pt hollow NPs were obtained. (d) The Au/Ag core/shell NPs were synthesized via the following procedures. First, 4 mL of sodium citrate (1 wt %) and 0.5 mL of 0.1 M $AgNO_3$ were added into the above 13 nm gold NPs solution (15 mL). Second, 4 mL of 0.1 M AA was added dropwise into the above solution and stirred for 30 min.

**2.5. Constructing Coaxial Nanocable/Metal Hybrid Nanostructures.** (a) The CNT/silica/metal hybrid nanostructures were prepared via mixing 1 mL of APTMS-functionalized CNT/silica coaxial nanocable aqueous solution with 10−20 mL of gold or hollow Pt or Au/Pt hybrid NPs or Au/Ag core/shell NPs solutions (slight excess). The resulting products were collected via centrifugation and dissolved in water. (b) For synthesis of CNT/silica/(Au/Ag) hybrid materials, we can also use CNT/silica/Au hybrid material as a seed. For example, 1 mL of CNT/silica/Au hybrid material was added into 19 mL of water, followed by the addition of 4 mL of sodium citrate (1 wt %) and 0.5 mL of 0.1 M $AgNO_3$. Then, 4 mL of 0.1 M AA was added dropwise into the above solution and stirred for 30 min. Finally, the solution was centrifuged and dissolved in 4 mL of water.

**2.6. Electrocatalytic Experiments.** The electrode was loaded with CNT/silica/Au/Pt hybrid nanomaterial (5 $\mu$L). Electrocatalytic oxygen reduction measurements were carried out in a 0.5 M $H_2SO_4$ solution. Electrocatalytic methanol oxidation measurements were carried out in a 0.5 M $H_2SO_4$ solution containing 1 M methanol. For RRDE voltammetry experiments, 10 $\mu$L of the hybrid material solution was dropped onto the GC electrode (5 mm) and allowed to dry at room temperature. Then, 5 $\mu$L of Nafion (0.25%) solution was placed on the surface of the above modified electrode. All other electrochemical experiments were carried out in a 0.1 M phosphate buffer solution (PBS, pH 7.0).

**2.7. SERS Measurements.** For SERS studies, 20 $\mu$L of Au/Ag core/shell NPs aggregates supported on coaxial nanocable or Au/Ag core/shell NPs aqueous solution was dropped onto the glass substrate and dried at ambient condition, and then 20 $\mu$L of $2.0 \times 10^{-4}$ M 4-ATP ethanol solution or $10^{-4}$ M adenine aqueous solution was dropped onto the corresponding nanostructure film for drying. After washing of glass substrate with ethanol and drying by $N_2$, SERS spectra were recorded under ambient conditions.

## 3. Results and Discussion

**3.1. Synthesis and Characterization of Hybrid Materials.** The whole preparation strategy for constructing diverse metal NPs/coaxial nanocable composite nanostructures is

(17) (a) Wang, Y.; Wei, H.; Li, B.; Ren, W.; Guo, S.; Dong, S.; Wang, E. *Chem. Commun.* **2007**, 5220. (b) Guo, S.; Wang, L.; Dong, S.; Wang, E. *J. Phys. Chem. C* **2008**, *112*, 13510. (c) Guo, S.; Li, J.; Wang, E. *Chem. Asian J.* **2008**, *3*, 1544.

**Scheme 1. Procedure To Design Diverse Metal NPs/Coaxial Nanocable Composite Nanostructures**

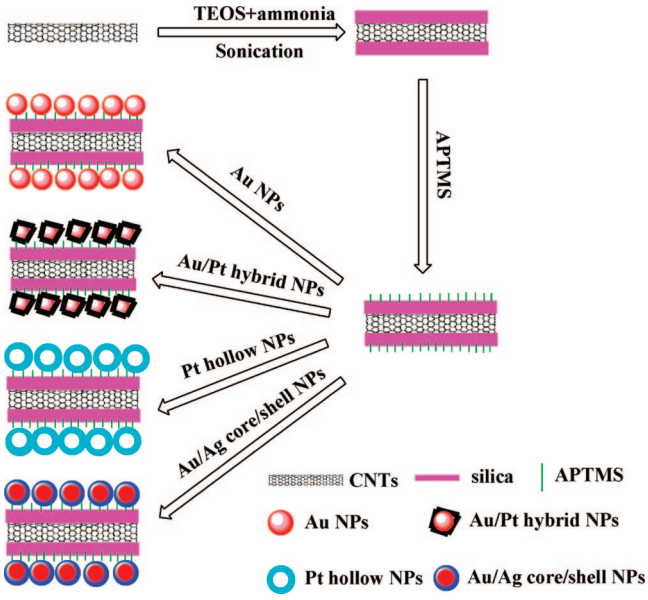


shown in Scheme 1. The structure and morphology of the CNT/$SiO_2$ coaxial nanocables obtained were characterized using SEM and TEM. Figure 1A,B shows typical SEM images of the as-made coaxial nanocables at different magnifications. A great number of 1D nanofibers with a diameter of 100−140 nm are observed. A high-magnification image (Figure 1B) shows that very homogeneous silica layers are coated on the surface of the CNTs. Note that the diameter of the CNT was in the range 20−50 nm, which further proves the fact that CNT/$SiO_2$ coaxial nanocables were obtained. Figure 1C shows a typical TEM image of coaxial nanocables. A contrast difference in coaxial nanocables with a lighter center surrounded by a darker edge is observed, confirming their core/shell structure. Actually, the thickness of $SiO_2$ on the surface of CNTs (data not shown) could be easily controlled by changing the weight ratio of CNT to tetraethoxysilane (TEOS) or by using as-prepared coaxial nanocable as a seed.

It is interesting to note that after functionalization with a $NH_2$ group, coaxial nanocables could easily adsorb ultrahigh-density metal nanomaterials. Figure 2A shows a typical SEM image of CNT/$SiO_2$/(Au/Pt) hybrid nanostructures. Compared with the CNT/$SiO_2$ coaxial nanocable (Figure 1B), the CNT/$SiO_2$/(Au/Pt) hybrid nanostructures have a rougher surface, indicating that small Au/Pt NPs have been adsorbed on the surface of coaxial nanocables. To reveal the detailed structure of CNT/$SiO_2$/(Au/Pt) hybrid nanomaterials, the corresponding TEM images are shown in Figure 2B,C. A large number of Au/Pt NPs with a diameter of about 7 nm are found, indicating the feasibility of our methods. The energy-dispersive X-ray (EDX) spectroscopy pattern (Figure 3A) indicates that the above hybrid nanomaterials are composed of the elements gold, platinum, silicon, and carbon (other signals are from the substrate). To further confirm the existence of Au, Pt, silica, and CNTs in the resulting UASCN, an XPS experiment was employed for the surface analysis of the above sample. XPS patterns of the resulting UASCN show a significant Au(4f) signal corresponding to the binding energy of metallic Au (Figure 3B), a Pt(4f) signal characteristic of metallic Pt (Figure 3C), a C(1s) signal characteristic of CNT (Figure 3D), and Si(2p) signal characteristic of silica (Figure 3E). Thus, we can affirm that Au/Pt hybrid NPs supported on coaxial nanocables could be easily obtained via the previous method. More interestingly, the present functionalization strategy is also a general and attractive method for the decoration of coaxial nanocables with size-, shape-, and composition-controlled metal NPs. For example, Au NPs (Figure 4A), Pt hollow NPs (Figure 4B,C), and Au/Ag core/shell NPs (Figure 4D,E) could also be easily adsorbed on the surface of coaxial nanocables. We have compared the electrochemical activity of UASCN with that of Pt hollow NPs supported on coaxial nanocables. A comparison of hydrogen adsorption/desorption and metal oxidation/reduction events of these catalysts indicates that the UASCN exhibited slightly higher electrochemical activity than that of Pt hollow NPs supported on coaxial nanocables (data not shown), which was caused by the fact that UASCN has very high density, small Au/Pt NPs.

**3.2. Oxygen Electrocatalytic Reduction.** The oxygen reduction reaction (ORR) is a reaction of indispensable importance in metal−air batteries and fuel cells and in oxygen sensors. The electroreduction of oxygen usually requires high current density, low overpotential, and nearly synchronous delivery of four electrons. A great number of electrocatalysts with individual components have exhibited high electrocatalytic activity toward ORR. However, compared with the existed catalysts, the present CNT/$SiO_2$/Au/Pt hybrid nanostructures have obvious advantages. First, Au/Pt hybrid NPs will reduce the cost of expensive Pt and in the meantime maintain their high electrocatalytic activity, as shown in ref 18. Second, ultra-high-density Au/Pt hybrid NPs supported on a 3D coaxial nanocable will further increase the efficient electrochemical active area. Figure 5A shows the typical cyclic voltammograms (CVs) of oxygen reduction at the hybrid-materials-modified GCE in a 0.5 M $H_2SO_4$ solution in the presence of air (line d) and $N_2$ (line b). In the presence of air, a remarkable catalytic reduction current occurs at 0.42 V (line d) at a scan rate of 50 mV/s while no catalytic reduction current could be observed at the bare GCE (line a) and hybrid-materials-modified electrode in the presence of $N_2$ (line b) in the potential range employed. This indicates that the electrocatalytic current located at 0.42 V (vs Ag/AgCl) could be ascribed to the reduction current of oxygen. Electrocatalytic oxygen reduction on a GCE modifed by Au/Pt hybrid NPs was also investigated, as shown in Figure 5A (line c). It is found that the as-prepared Au/Pt hybrid NPs exhibited lower current than that of hybrid materials, indicating that the UASCN have higher electrocatalytic activity. Note that the reduction potential (0.42 V) observed at the hybrid-materials-modified electrode is significantly more positive than the other Pt-based electrodes.[19] For instance, Dong's group studied the electrocatalytic reduction of oxygen at Pt-coated Au particle

(18) Guo, S.; Wang, L.; Dong, S.; Wang, E. *J. Phys. Chem. C* **2008**, *112*, 13510.
(19) (a) Jin, Y.; Shen, Y.; Dong, S. *J. Phys. Chem. B* **2004**, *108*, 8142. (b) Ye, H.; Crooks, R. M. *J. Am. Chem. Soc.* **2005**, *127*, 4930.

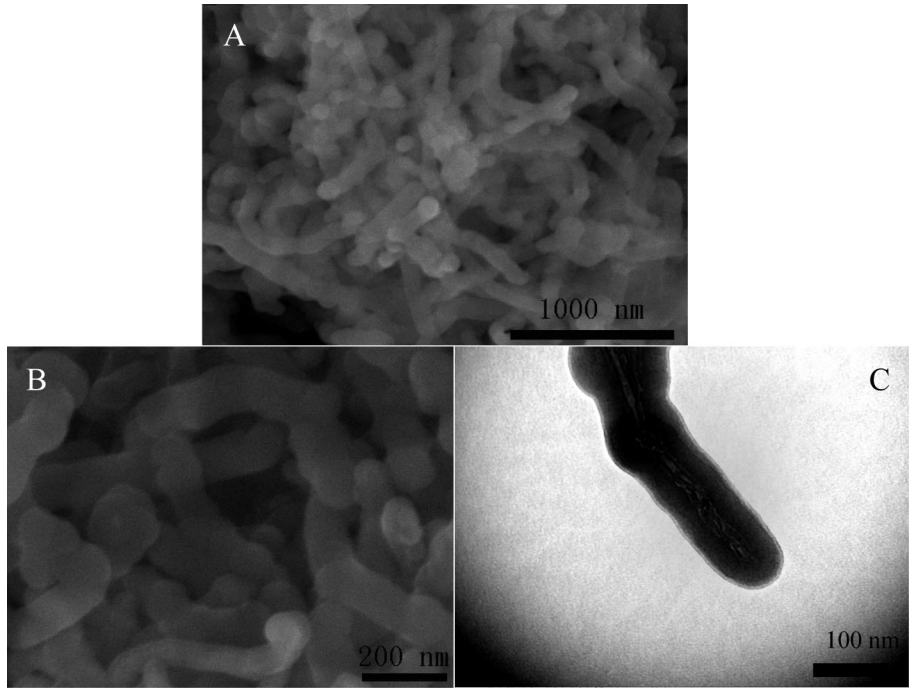


**Figure 1.** Typical SEM (A,B) images of CNT/silica coaxial nanocables at different magnifications. Typical TEM (C) image of CNT/silica coaxial nanocables.

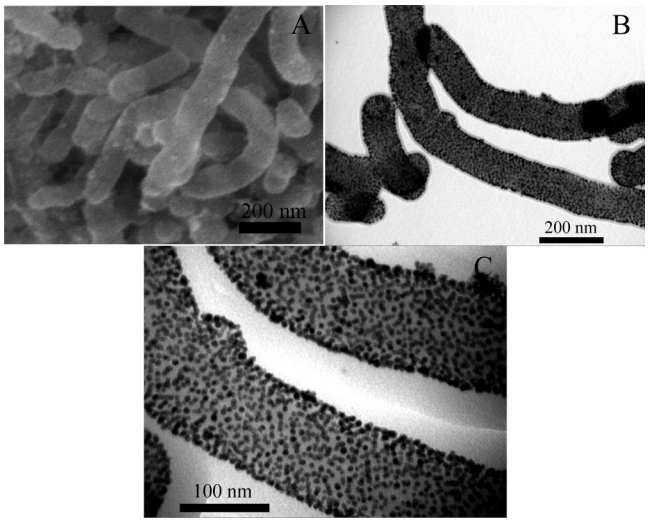


**Figure 2.** Typical SEM (A) image of Au/Pt hybrid NPs supported on coaxial nanocables. Typical TEM (B,C) images of Au/Pt hybrid NPs supported on coaxial nanocables at different magnifications.

and the reduction of oxygen at ~0.1 V (Ag/AgCl) was observed.[19a] Crooks and co-worker reported that the dendrimer-encapsulated Pt-NPs-modified electrode shows the reduction peak at ~0.25 V.[19b] These further reveal that the present UASCN-modified electrode has good electrocatalytic activity toward ORR.

The additional important index is the four-electron electroreduction of oxygen to water, which is the reaction greatly pursued by scientists in view of its important application in fuel cells. So the hybrid-materials-modified GCE was further investigated by rotating disk electrode (RDE) and rotating ring-disk electrode (RRDE) experiments. Depicted in Figure 5B are current−potential curves of oxygen reduction at a RDE catalyzed by UASCN with different rotating rates in an air-saturated 0.5 M $H_2SO_4$ solution. The corresponding Levich and Koutecky−Levich plots were also obtained. From the slope of the Koutecky−Levich plot, the $n$ (the electron-transfer number) value was evaluated to be about 4 for a UASCN-modified electrode. The excellent electrocatalytic ability of hybrid materials for four-electron electroreduction of oxygen was also testified by a RRDE study. Figure 5C shows the voltammetric curves for oxygen reduction, recorded at the RRDE with UASCN immobilized on the GCE. In this experiment, the disk potential was scanned from +1.0 to 0.1 V, while the ring potential was kept at +1.0 V to detect any $H_2O_2$ evolved at the disk electrode. A large disk current was obtained, whereas an almost negligible ring current was observed, which suggests that the as-prepared hybrid electrocatalyst reduced oxygen by almost four electrons to $H_2O$. From the ratio of the ring-disk current, the electron-transfer number ($n$) was calculated to be about 4 according to the equation $n = 4 - 2(I_R/I_D N)$.[1d]

**3.3. Methanol Electrocatalytic Oxidation.** Another important electrocatalytic reaction that is deeply studied by scientists is the methanol oxidation reaction (MOR). Herein, the electrocatalytic activity of UASCN toward MOR was also tested. The measurements were carried out in a 0.5 M $H_2SO_4$ aqueous solution containing 1.0 M methanol. A GC electrode with a diameter of about 3 mm was used as the working electrode. Figure 6A shows the voltammetry curves of bare GCE (line a) and GCEs modified by CNT/silica coaxial nanocables (line b), UASCN (line c), and Au/Pt hybrid NPs (line d), in a 0.5 M $H_2SO_4$ solution containing 1 M methanol. It is found that the UASCN-modified GCE (line c) exhibited higher current than that of Au/Pt hybrid NPs (line d), which can be ascribed to the fact that coaxial nanocables probably act as a 3D support for effectively increasing the electrochemical activity area. In addition, the ratio of the forward oxidation current peak ($I_f$) to the

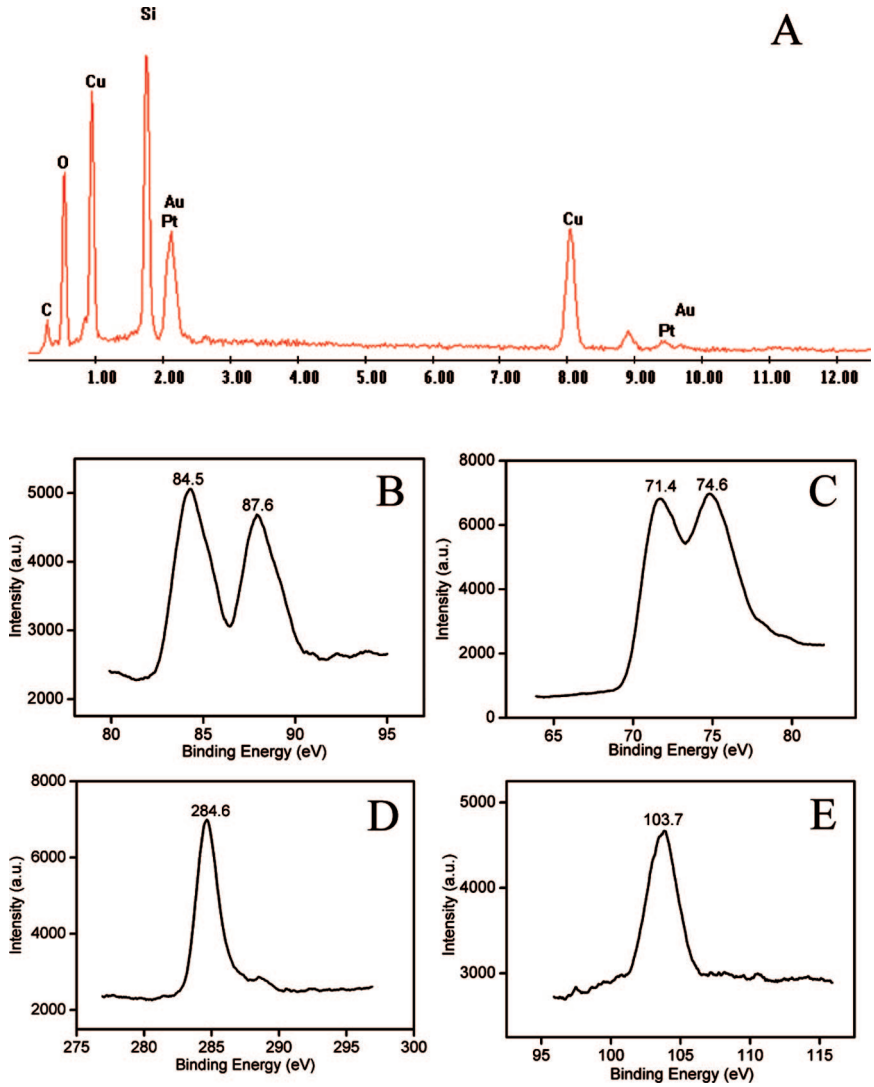


**Figure 3.** EDX (A) and XPS (B−E) patterns of Au/Pt hybrid NPs supported on coaxial nanocables. (B) Au(4f); (C) Pt(4f); (D) C(1s); (E) Si(2p).

reverse current peak ($I_b$), $I_f/I_b$, is an index of the catalyst tolerance to the poisoning species.[13b] A higher ratio indicates more effective removal of the poisoning species on the catalyst surface. The $I_f/I_b$ ratio of UASCN is about 2, which is higher than that of the E-TEK catalyst (0.74),[13b] showing better catalyst tolerance of hybrid materials. Furthermore, the electrocatalytic behavior of UASCN-modified GCE toward $CH_3OH$ was studied further with the change of scan rate. As shown in Figure 6B, when the scan rate increases from 0.01 to 0.2 V/s, the anodic peak currents increase. The peak current increases linearly with the square root of the scan rate in the range of 0.01−0.2 V/s (data not shown), indicating it was a diffusion-controlled process.

**3.4. Direct Detection of Hydrogen Peroxide.** The reliable, accurate, and rapid determination of $H_2O_2$ is of practical importance because it is an essential mediator in food, pharmaceutical, clinical, industrial, and environmental analyses.[20] A large number of biosensors based on the electrocatalysis of immobilized enzymes to $H_2O_2$ reduction were developed to detect $H_2O_2$.[21,22] However, the enzymes were relatively expensive and critical about the environmental conditions. Furthermore, the enzymes cannot obviously provide the biosensors with a complete long-term stability because of their inherent instability. The immobilization of a mediator such as ferrocene derivatives into an electrochemical sensing interface for amperometric detection of peroxides is of great interest.[23] But leakage has been the main problem for the entrapment of a low molecular weight mediator when introduced to the electrochemical interface. Therefore, it is very necessary to develop a simple enzymeless and mediator-less strategy for highly sensitive sensing $H_2O_2$. The present UASCN-modified GCE provides a good opportunity to build a highly sensitive $H_2O_2$ electrochemical sensor. Figure 7A shows the CVs of bare GCE (line a) and GCEs modified by Au/Pt hybrid NPs (line c) and UASCN (lines b, d), in the absence (line b) and presence of 1 mM

(20) Wolfbeis, O.; Drkop, A.; Wu, M.; Lin, Z. *Angew. Chem., Int. Ed.* **2002**, *41*, 4495.
(21) Jia, J.; Wang, B.; Wu, A.; Cheng, G.; Li, Z.; Dong, S. *Anal. Chem.* **2002**, *74*, 2217.
(22) Guo, S.; Wang, E. *Anal. Chim. Acta* **2007**, *598*, 181.
(23) Tripathi, V. S.; Kandimalla, V. B.; Ju, H. *Biosens. Bioelectron.* **2006**, *21*, 1529.

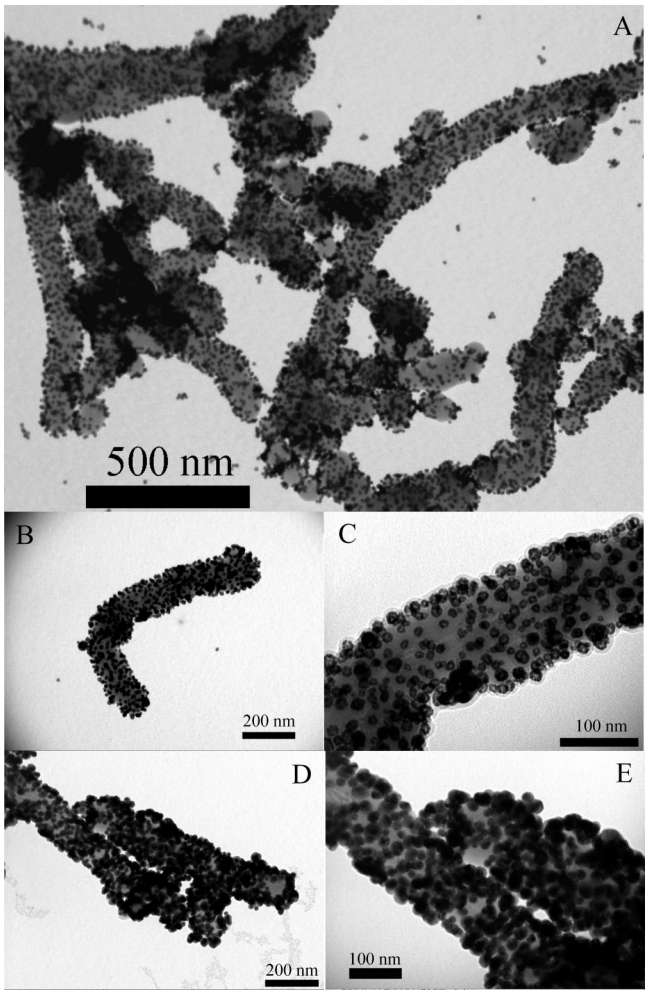


**Figure 4.** Typical TEM (A) image of Au NPs supported on coaxial nanocables. Typical TEM (B,C) images of hollow Pt NPs supported on coaxial nanocables at different magnifications. Typical TEM (D,E) images of Au/Ag core/shell NPs supported on coaxial nanocables at different magnifications.

$H_2O_2$ (lines a, c, d) in 0.1 M PBS (pH 7.0). From Figure 7A (line d), it is observed that an obvious peak current occurs at −0.15 V while no reduction peaks of $H_2O_2$ were observed at the bare GCE (line a). In particular, the UASCN-modified GCE exhibited higher catalytic current than that of Au/Pt hybrid NPs, indicating that the UASCN-modified electrode showed better electrocatalytic activity toward $H_2O_2$ reduction. Figure 7B shows the CVs of UASCN-modified GCE in the presence of $H_2O_2$ with different concentrations. With increasing the concentration of $H_2O_2$ (from top to bottom: 0, 0.1, 0.3, 0.5, 0.7, 1, and 1.5 mM), the $H_2O_2$ reduction currents gradually increase. Furthermore, the electrocatalytic behavior of the UASCN-modified electrode toward $H_2O_2$ was studied further with the change of scan rate. As shown in Figure 7C, when the scan rate increases from 0.02 to 0.2 V/s, the cathodic peak currents increase. The peak currents increase linearly with the square root of the scan rate in the range of 0.02−0.2 V/s (data not shown), indicating it was a diffusion-controlled process.

Figure 7D shows a typical amperometric response of the UASCN-modified electrode on successive addition of $H_2O_2$ into stirring 0.1 M PBS (pH 7.0) at an applied potential of −0.1 V. As $H_2O_2$ was added into the stirring buffer solution, the modified electrode responded rapidly to the substrate. The prepared sensor could achieve the maximum steady-state current within 3.5 s. The fast response could be attributed to the fact that $H_2O_2$ can rapidly diffuse into the UASCN freely because of the particular structure of UASCN as demonstrated in Figure 2C. The modified electrode exhibited sensitive response to $H_2O_2$ with a linear range from 0.5 $\mu$M to 1.67 mM (Figure 7E) and a detection limit of 0.3 $\mu$M based on S/N = 3, which was lower than certain HRP-based biosensors[24,25] and $H_2O_2$ sensors based on functional nanomaterials such as a gold nanowire assembling sphere[26] and mesoporous Pt,[27] and was comparable to $H_2O_2$ sensors based on hybrid nanomaterials such as Pd NPs supported on carbon nanofibers[12] and Pt NPs supported on CNTs.[28] The above comparison data reveal that the as-prepared UASCN has good electrocatalytic activity toward $H_2O_2$.

The selectivity of the UASCN for the detection of $H_2O_2$ was also evaluated. Figure 7F shows the current responses of the UASCN to the electroactive interferences of AA (0.2 mM) and UA (0.35 mM). This concentration was selected because the level of endogenous AA and UA is respectively about 0.125 mM and 0.33 mM in blood samples.[12] As can be seen, the current responses of AA and UA observed were much smaller than those of $H_2O_2$, indicating that our UASCN has excellent selectivity for the detection of $H_2O_2$.

**3.5. Detection of Hydrazine.** Hydrazine is widely used as a fuel in rocket propulsion systems and used in missile systems, fuel cells, pesticides, photography chemicals, weapons for mass destruction, and so on.[29,30] It is a neurotoxin and hence produces carcinogenic and mutagenic effects, causing damage to the lungs, liver, and kidneys. Therefore, it is highly desirable to fabricate a reliable and sensitive analytical tool for the effective detection of hydrazine. The rapid development of nanoscience and nanotechnology provides a good opportunity for developing highly sensitive electrochemical devices for effective detection of hydrazine. CNT, ZnO, and other novel nanomaterials have exhibited high electrocatalytic activity toward hydrazine oxidation.[31,32] However, to the best of our knowledge, there are no reports on the exploration of ultra-high-density Au/Pt hybrid NPs supported on CNT/silica coaxial nanocables as enhanced materials for constructing hydrazine electrochemical sensors.

Figure 8A shows CVs of the bare GCE (line b) and GCEs modified by Au/Pt hybrid NPs (line c) and UASCN (lines

(24) Chen, H.; Dong, S. *Biosens. Bioelectron.* **2007**, *22*, 1811.
(25) Lei, C.; Hu, S.; Gao, N.; Shen, G.; Yu, R. *Bioelectrochemistry* **2004**, *65*, 33.
(26) Guo, S.; Wen, D.; Dong, S.; Wang, E. *Talanta* **2009**, *77*, 1510.
(27) Evans, S. A. G.; Elliott, J. M.; Andrews, L. M.; Bartlett, P. N.; Doyle, P. J.; Denuault, G. *Anal. Chem.* **2002**, *74*, 1322.
(28) Zou, Y.; Xiang, C.; Sun, L.-X.; Xu, F. *Biosens. Bioelectron.* **2008**, *23*, 1010.
(29) Garrod, S.; Bollard, M. E.; Nicholls, A. W.; Connor, S. C.; Connelly, J.; Nicholson, J. K.; Holmes, E. *Chem. Res. Toxicol.* **2005**, *18*, 115.
(30) Narayanan, S. S.; Scholz, F. *Electroanal.* **1999**, *11*, 465.
(31) (a) Lin, Y.; Lu, F.; Tu, Y.; Ren, Z. *Nano Lett.* **2004**, *4*, 191. (b) Mukhopadhyay, K.; Phadtare, S.; Vinod, V. P.; Kumar, A.; Rao, M.; Chaudhari, R. V.; Sastry, M. *Langmuir* **2003**, *19*, 3858. (c) Azamian, B. R.; Davis, J. J.; Coleman, K. S.; Bagshaw, C. B.; Green, M. L. H. *J. Am. Chem. Soc.* **2002**, *124*, 12664.
(32) Umar, A.; Rahman, M. M.; Kim, S. H.; Hahn, Y. *Chem. Commun.* **2008**, 166.

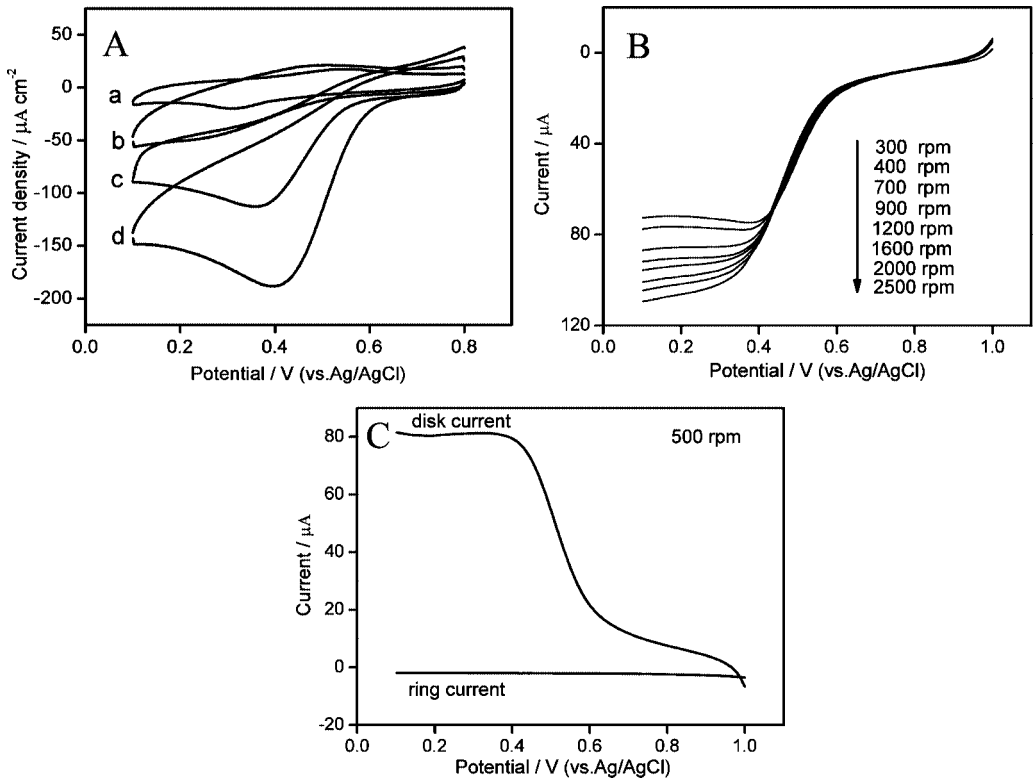


**Figure 5.** (A) CVs of $O_2$ reduction at the bare GCE (a), UASCN-modified GCE (b and d), and Au/Pt hybrid NPs (c) in air-saturated (a, c, d) and $N_2$-saturated (b) 0.5 M $H_2SO_4$ solutions. (B) Current−potential curves of $O_2$ reduction at a UASCN-modified rotating disk electrode with different rotating rates in an air-saturated 0.5 M $H_2SO_4$ solution. (C) Current−potential curves of $O_2$ reduction at a UASCN-modified rotating ring-disk electrode in an air-saturated 0.5 M $H_2SO_4$ solution. The potential of the ring electrode was set at 1.0 V; the rotation rate was 500 rpm. All the scan rates were 50 mV/s.

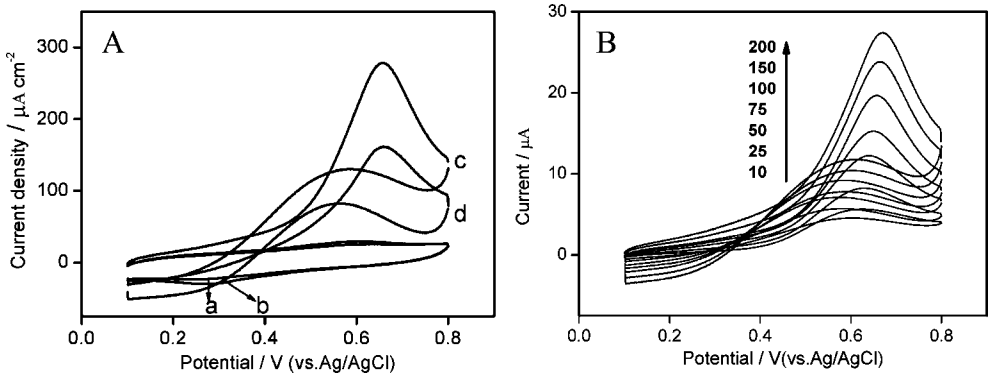


**Figure 6.** (A) CVs of methanol oxidation at the bare GCE (a) and GCEs modified by CNT/$SiO_2$ (b), UASCN (c), and Au/Pt hybrid NPs (d), in 0.5 M $H_2SO_4$ solutions containing 1 M methanol. The scan rate was 100 mV/s. (B) CVs of methanol oxidation at the UASCN-modified GCE in 0.5 M $H_2SO_4$ solution containing 1 M methanol at different scan rates.

a, d), in the absence (line a) and presence of 1 mM $N_2H_4$ (lines b, c, d) in 0.1 M PBS (pH 7.0). It can be observed that in contrast to the UASCN-modified electrode without hydrazine (line a), a well-defined oxidation peak with 1 mM $N_2H_4$ in 0.1 M PBS (line c) is observed with a peak potential of −0.1 V, which is more negative than that found in the existing literature.[32] Also, the UASCN-modified electrode exhibited higher catalytic current than that of Au/Pt hybrid NPs. Both indicate that the present UASCN-modified electrode exhibited high electrocatalytic activity toward hydrazine oxidation reaction. Figure 8B shows the CVs of hybrid-materials-modified GCE in the presence of hydrazine with different concentrations (from bottom to top: 1, 2, 3, 4, 5, 8, and 10 mM). When the concentration of hydrazine increases, the hydrazine oxidation currents gradually increase. Furthermore, the electrocatalytic behavior of the UASCN-modified electrode to hydrazine was studied further with the change of scan rate. As shown in Figure 8C, when the scan rate increases from 0.01 to 0.2 V/s, the anodic peak currents increase. The peak currents increase linearly with the square root of the scan rate in the range of 0.01−0.2 V/s (data not shown), indicating it was a diffusion-controlled process. Figure 8D shows differential pulse stripping voltammetry (DPSV) of UASCN-modified GCE in the absence of hydrazine and presence of hydrazine with different concentrations (from bottom to top: 0, 0.5, 1, 3, 5, and 8 $\mu$M). It is found that when the concentration of hydrazine increases, the peak currents increase rapidly. Under the optimized conditions, the steady-state current showed a linear relationship with the hydrazine concentration in the range of 0.5−8 $\mu$M (Figure

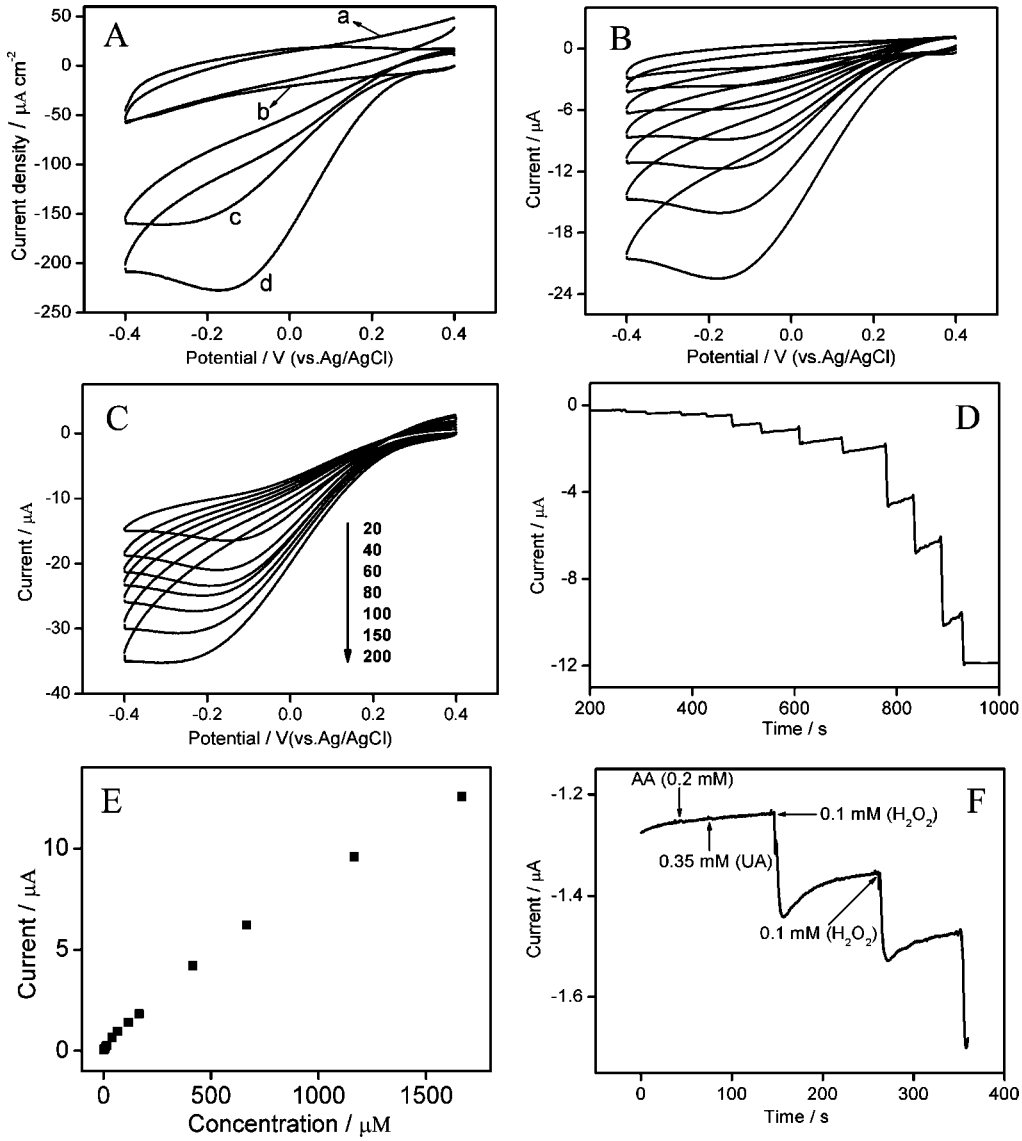


**Figure 7.** (A) CVs of $H_2O_2$ reduction at the bare GCE (a) and GCEs modified by Au/Pt hybrid NPs (c) and UASCN (b, d), in a 0.1 M PBS in the absence (b) and presence of 1 mM $H_2O_2$ (a, c, d). The scan rate was 50 mV/s. (B) CVs of $H_2O_2$ reduction at the UASCN-modified GCEs in a 0.1 M PBS in the presence of $H_2O_2$ with different concentrations (from top to bottom: 0, 0.1, 0.3, 0.5, 0.7, 1, and 1.5 mM). The scan rate was 50 mV/s. (C) CVs of $H_2O_2$ reduction at the UASCN-modified GCEs in a 0.1 M PBS containing 1.5 mM $H_2O_2$ at different scan rates. (D) Typical amperometric current response of the UASCN-modified electrode on successive injection of $H_2O_2$ into stirring $N_2$-saturated PBS (pH 7.0). Applied potential, −0.1 V. (E) Plot of the electrocatalytic current of $H_2O_2$ vs its concentrations. (F) Current responses of the UASCN to the sequential additions of 0.1 mM $H_2O_2$, 0.2 mM AA, and 0.35 mM UA into 0.1 M PBS.

8E). The detection limit is <0.5 $\mu$M with a signal-to-noise ratio of 3, which was lower than those of amperometric hydrazine sensors based on zinc oxide nanonails,[32] CNTs-modified electrodes,[33] *o*-aminophenol grafted GCE electrode,[34] multilayer film containing cobalt phthalocyanine,[35] etc. Therefore, one can conclude that the present hybrid material is a good candidate for the fabrication of efficient and highly sensitive hydrazine sensors.

**3.6. SERS Activity of Au/Ag Core/Shell NPs Supported on Coaxial Nanocables.** It would be interesting to explore the possibile use of the as-prepared hybrid nanomaterial containing the aggregated Au/Ag core/shell NPs for fabricating intense SERS substrates to detect different molecules. Figure 9(line b) depicts the SERS spectrum of 4-ATP molecules absorbed on the surface of CNT/$SiO_2$/(Au/Ag) hybrid nanomaterial. Compared with the normal Raman spectrum of solid 4-ATP (Figure 9, line a), noticeable changes in the frequency shift can be observed from the SERS spectra on the above hybrid-material-modified substrates, indicating that the thiol group in 4-ATP directly contacts the silver surfaces.[36] Two sets of bands were observed on the SERS spectra of 4-ATP on the assembling film: one set is located at 1077 $cm^{-1}$, which is assigned to the $a_1$ vibration modes, and the other set is located at 1140, 1389, 1435, and 1575 $cm^{-1}$, which are assigned to the $b_2$ vibration modes.[37] As reported by Osawa et al.,[38] the enhancement of $b_2$ modes is attributed to the chemical

(33) Zare, H. R.; Nasirrizadeh, N. *Electrochim. Acta* **2007**, *52*, 4153.
(34) Nassef, H. M.; Radi, A. E.; O'Sullivan, C. K. *J. Electroanal. Chem.* **2006**, *592*, 139.
(35) Sun, C.; Sun, Y.; Zhang, X.; Zhang, X.; Jian, D.; Gao, Q.; Xu, H.; Shen, J. *Thin Solid Films* **1996**, *288*, 291.
(36) Wei, G.; Wang, L.; Liu, Z.; Song, Y.; Sun, L.; Yang, Y.; Li, Z. *J. Phys. Chem. B* **2005**, *109*, 23941.
(37) Zheng, J. W.; Li, X. W.; Ji, Y.; Gu, R. A.; Lu, T. H. *J. Phys. Chem. B* **2002**, *106*, 1019.

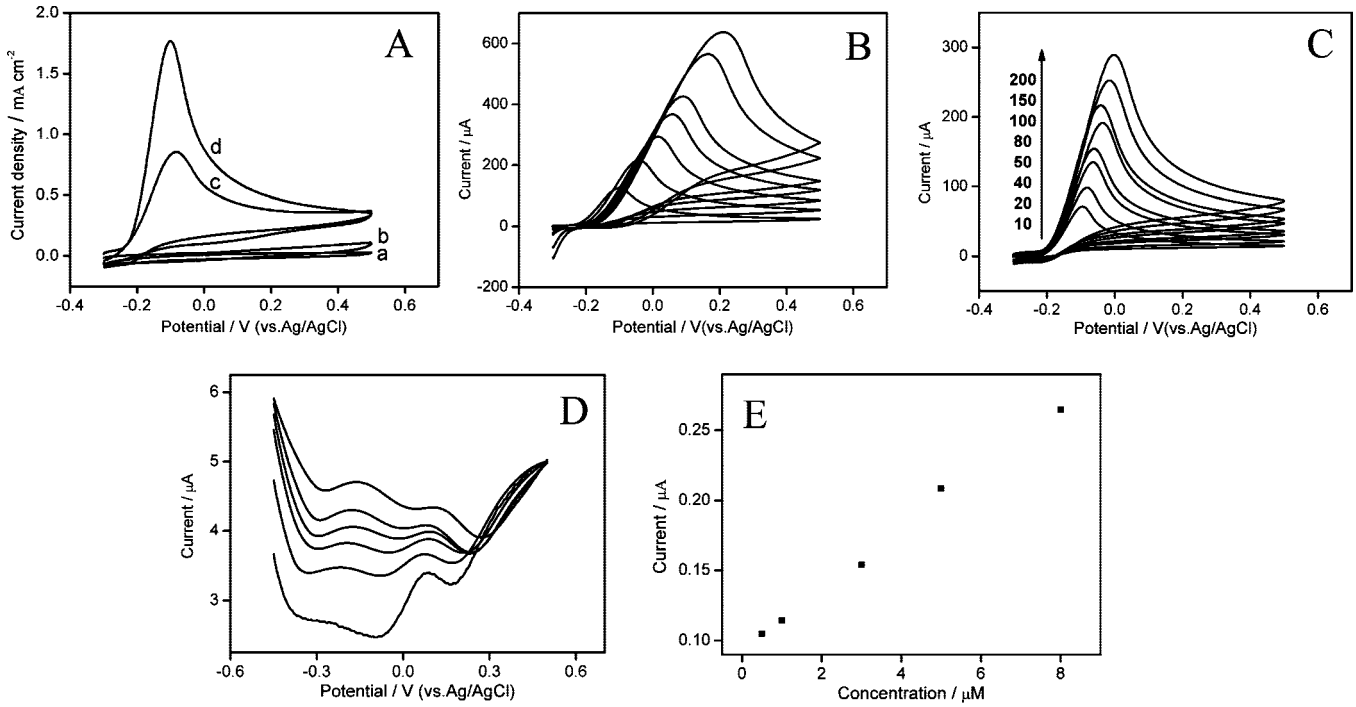


**Figure 8.** (A) CVs of hydrazine oxidation at the bare GCE (b) and GCEs modified by UASCN (a, d) and Au/Pt hybrid NPs (c), in a 0.1 M PBS solution in the absence (a) and presence (b, c, d) of 1 mM hydrazine. The scan rate was 100 mV/s. (B) CVs of hydrazine oxidation at the UASCN-modified GCEs in a 0.1 M PBS in the presence of hydrazine with different concentrations (from bottom to top: 1, 2, 3, 4, 5, 8, and 10 mM). Scan rate was 100 mV/s. (C) CVs of hydrazine oxidation at the UASCN-modified GCEs in 0.1 M PBS containing 2 mM hydrazine at different scan rates. (D) DPSV of UASCN-modified GCE in the presence of hydrazine with different concentrations (from bottom to top: 0, 0.5, 1, 3, 5, and 8 $\mu$M). The scan rate was 50 mV/s. (E) Plot of electrocatalytic current of hydrazine vs its concentrations.

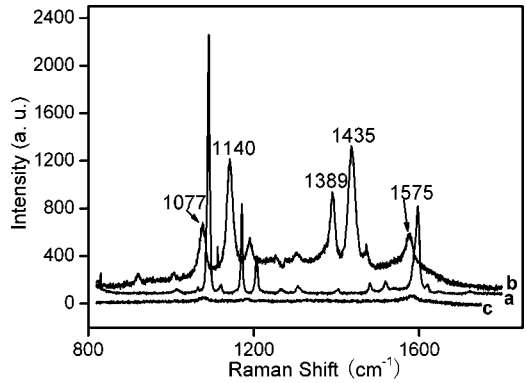


**Figure 9.** SERS spectrum of 4-ATP adsorbed on Au/Ag core/shell NPs (line c), Au/Ag core/shell NPs supported on coaxial nanocables (line b), and Raman spectrum of solid 4-ATP sample (line a).

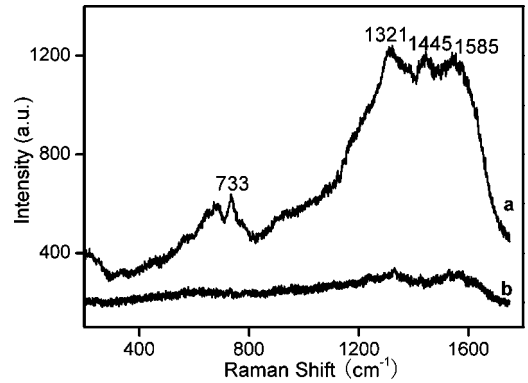


**Figure 10.** SERS spectra of adenine ($10^{-4}$ M) on the Au/Ag core/shell NPs supported on coaxial nanocables film (line a) and Au/Ag core shell NPs film (line b).

mechanism, most likely from the charge transfer (CT) of the adsorbate to the metal. Furthermore, it is found that substrates modified by CNT/$SiO_2$/(Au/Ag) hybrid materials exhibits much higher SERS activity (comparable intensity with Raman peak of solid 4-ATP) than that of individual Au/Ag core/shell NPs (Figure 9, line c). This is probably caused by the fact that the surface of CNT/$SiO_2$/(Au/Ag) hybrid materials had a great number of hot spots (clearance of Au/Ag hybrid NP aggregates), which is favorable for enhancing the SERS signals.[16,39]

Adenine was chosen as another target molecule because of its importance in the direct detection of nucleotide-based molecules for rapid DNA sequencing. The SERS spectrum of adenine ($10^{-4}$ M) was also tested to examine the viability of CNT/$SiO_2$/(Au/Ag) hybrid materials as a general SERS substrate, as shown in Figure 10 (line a). It is found that four vibrations at 733, 1321, 1445, and 1585 $cm^{-1}$ are pronounced, which are assigned to the purine ring breathing mode, the CN stretching mode, in-plane C−N stretching mode, and sciss $NH_2$, C−N stretching mode, respectively.[39,40] Compared with SERS of adenine on CNT/$SiO_2$/(Au/Ag) with that of Au/Ag core/shell NPs (Figure 10, line b), the CNT/$SiO_2$/(Au/Ag) exhibited much higher SERS activity, indicating the direct detection and identification of single native nucleotides should be possible because of the unique SERS

(38) Osawa, M.; Matsuda, N.; Yoshi, K.; Uchida, I. *J. Phys. Chem.* **1994**, *98*, 12702.
(39) Kneipp, K.; Kneipp, H.; Itzkan, I.; Dasari, R.; Feld, M. S. *Chem. Rev.* **1999**, *99*, 2957.
(40) Wang, Y.; Guo, S.; Chen, H.; Wang, W. *J. Colloid Interface Sci.* **2008**, *318*, 82.

spectra of their bases on the CNT/$SiO_2$/(Au/Ag) film. Thus, it is expected that the present hybrid materials will probably find potential applications in the field of detecting different target molecules using the SERS technique.

## Conclusions

We have successfully developed a very simple strategy for synthesizing well-defined CNT/silica coaxial nanocable. The as-obtained coaxial nanocable has been used as an advanced 3D support for loading diverse metal nanostructures. It is found that ultra-high-density metal nanomaterials such as gold NPs, Au/Pt hybrid NPs, Pt hollow NPs, and Au/Ag core/shell NPs could easily adsorb on the surface of CNT/silica coaxial nanocable. Furthermore, the present ultra-high-density Au/Pt NPs supported on coaxial nanocables could be used as enhanced materials for constructing different electrochemical devices with high performance for oxygen, methanol, $H_2O_2$, and hydrazine. It is also found that the as-obtained high-density Au/Ag core/shell NPs supported on coaxial nanocable could be used as a good SERS substrate for the detection of different molecules (4-ATP and adenine), showing the great potential of CNT/$SiO_2$/(Au/Ag) as a convenient and powerful SERS substrate for biological tags and biological molecular detection. It is expected that the above hybrid materials will probably find applications in other important fields such as electronics, biomedicine, and biosensors.

**Acknowledgment.** This work was supported by the National Natural Science Foundation of China (Nos. 20675076, 20735003, and 20820102037) and the National High Technical Development Project (863 Project) Foundation of China (2007AA061501) and the 973 Project (Nos. 2007CB714500 and 2009CB930100).

CM900300V